RF-MEMS Switches for Reconfigurable Integrated Circuits

Elliott R. Brown, *Senior Member, IEEE*

(Invited Paper)

***Abstract*— This paper deals with a relatively new area of radio-frequency (RF) technology based on microelectromechanical systems (MEMS). RF MEMS provides a class of new devices and components which display superior high-frequency performance relative to conventional (usually semiconductor) devices, and which enable new system capabilities. In addition, MEMS devices are designed and fabricated by techniques similar to those of very large-scale integration, and can be manufactured by traditional batch-processing methods. In this paper, the only device addressed is the electrostatic microswitch—perhaps the paradigm RF-MEMS device. Through its superior performance characteristics, the microswitch is being developed in a number of existing circuits and systems, including radio front-ends, capacitor banks, and time-delay networks. The superior performance combined with ultra-low-power dissipation and large-scale integration should enable new system functionality as well. Two possibilities addressed here are quasi-optical beam steering and electrically reconfigurable antennas.**

I. Introduction

THE 1990's have brought a profound change in radio-frequency (RF) technology driven largely by economic and geopolitical events. On one hand, the wind-down of the cold war has reduced the need for advanced RF systems, particularly sensors; on the other hand, the dawning of the information age has created a heightened interest and worldwide market for communications systems and networking of voice and data alike. The transition of RF technology from one era to the other has been both challenging and opportunistic. For the RF systems engineers, it has meant a shift of thinking from large centralized systems to smaller distributed systems. Along with this shift has come a change from long-range systems, having large RF transmit power, to shorter range systems, having relatively modest RF power. In many cases, the new smaller systems must be mobile or hand-held. The paradigm for these new systems is the cellular wireless network consisting of a single powerful base station feeding a local cell of hand sets acting like individual terminals or nodes of the network. The popular digital cellular and personal communications service (PCS) bands around 0.9 and 1.9 GHz, respectively, comprise much of the frequency spectrum being used for cellular purposes.

Manuscript received August 7, 1998; revised August 26, 1998.

The author was with DARPA Electronics Technology Office, Arlington, VA 22203 USA. He is now with the Electrical Engineering Department, University of California at Los Angeles, Los Angeles, CA 90095-1594 USA.

Publisher Item Identifier S 0018-9480(98)08402-6.

For technology engineers, the transition has been no less challenging. The premium devices and components formerly required to construct powerful centralized systems are no longer required or can no longer be afforded in many new distributed systems coming on line today. Instead, there is an emphasis on more affordable and integrable technology, which allows a greater degree of RF functionality per unit volume, even if at a lower level of performance than obtained with the former technologies. This has spawned widespread research and development of silicon-based RF integrated circuits (RFIC's), including deep-submicrometer Si CMOS and SiGe heterojunction bipolar transistors (HBT's). Taking advantage of the inherent manufacturability of Si very large-scale integration (VLSI), RFIC technology has found unique circuit and subsystem architectures well outside the traditional digital design. One example of this is the "RF system-on-a-chip," such as the family of integrated circuits (IC's) now commercially available for global positioning receivers.[1]

This paper deals with another technology that has emerged in recent years with a comparable level of interest and more rapid development than RFIC's. The technology is the design and fabrication of microelectromechanical systems (MEMS) for RF circuits (RF MEMS). In some ways, MEMS represents the new revolution in microelectronics. It is similar to VLSI circuits in that it allows the execution of complex functions on a size scale orders of magnitude lower and at far less power than discrete circuits. However, MEMS enables this miniaturization on a class of sensors and transducers that traditionally were constructed on the model of a large, often cumbersome transducer or sensor coupled to a highly integrated VLSI readout circuit or processor. A good example of this is the MEMS accelerometer, now one of the largest single MEMS application through its incorporation in air bags [1]. At the same time, MEMS leverages VLSI through the use of common design and batch processing methodologies and tools. It is this commonality with VLSI that has been credited to a large extent for the rapid dissemination of MEMS into the commercial marketplace.

It is important to realize up front that RF MEMS does not necessarily imply that the micromechanical system is operating at RF frequencies. As will be discussed briefly, in the largest class of RF MEMS devices and components, the microelectromechanical operation is used simply for the actuation or

[1] SIRF, Inc., Santa Clara, CA 95054 (e-mail: www.sirf.com).

adjustment of a separate RF device or component, such as a variable capacitor. In many of these devices, a key advantage of the MEMS devices compared to traditional semiconductor devices is electromechanical isolation. By this, we mean that the RF circuit does not leak or couple significantly to the actuation circuit. A second advantage is power consumption. Many of the RF MEMS devices under development carry out electromechanical coupling electrostatically through air (or vacuum). Hence, the power consumption comes from dynamic current flowing to the MEMS only when actuation is occurring.

However, the implementation of RF MEMS does not come with impunity. Due to the mechanical actuation, they are inherently slower than electronic switches. The electromechanical actuation time is typically many microseconds or greater, which is substantially longer than typical electrical time constants in semiconductor devices. In addition, RF MEMS devices can exhibit the phenomenon of "stiction," whereby parts of the device can bonded together upon physical contact. Each of these issues will be discussed further.

II. MEMS and Micromachining

According to a recent definition, a MEMS is a miniature device or an array of devices combining electrical and mechanical components and fabricated with IC batch-processing techniques [2]. Critical to this definition is that MEMS has both device and fabrication aspects. There are several MEMS fabrication techniques currently in widespread use, including bulk micromachining, surface micromachining, fusion bonding, and LIGA, which is a composite fabrication procedure of lithography, electroforming, and molding. The most important technique for RF MEMS is surface micromachining. In short, surface micromachining consists of the deposition and lithographic patterning of various thin films, usually on Si substrates. Generally, the intent is to make one or more of the ("release") films freestanding over a selected part of the substrate, thereby able to undergo the mechanical motion or actuation characteristic of all MEMS. This is done by depositing a "sacrificial" film (or films) below the released one(s), which is removed in the last steps of the process by selective etchants. The variety of materials for the release and sacrificial layers is great, including many metals (Au, Al, etc.), ceramics (SiO_2 and Si_3N_4), and plastics (photoresist, polymethyl methacrylate (PMMA), etc.). Depending on the details of the MEMS process and the other materials in the thin-film stack, the release and sacrificial layers can be deposited by evaporation, sputtering, electrodeposition, or other methods.

Surface micromachining has been used for a long time, dating back to MEMS work of the 1960's at Westinghouse. A breakthrough in surface micromachining has come in the form of dry etching, particularly reactive-ion etching (RIE). By mixing reactive chemicals in a plasma discharge and adding a semiconductor wafer with thin films deposited on top, select materials on the surface can be etched away at useful high rates and with high levels of material selectivity. For example, chlorine-bearing compounds in a high-density plasma can yield nearly isotropic silicon etching with a selectivity of silicon-to-SiO_2 of better than $100:1$. By the same token, low-pressure plasma etching [e.g., inductively coupled plasma (ICP)] allows independent control of the ion density and energy.

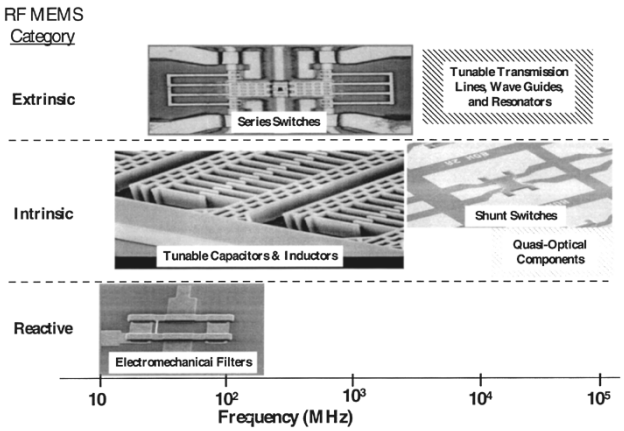

Fig. 1. Technology diagram for three different RF MEMS device categories.

Bulk micromachining involves the creation of mechanical structures directly in silicon, quartz, or other substrates by selectively removing the substrate material. It is the most mature of the micromachining technologies and has been used for many years in a variety of sensors and actuators, including pressure sensors, accelerometers, and ink-jet nozzles. The process includes the steps of wet chemical etching, RIE, or both to form the released or stationary microstructures. With wet etching, the resulting structures depend on the directionality of the etch, which is a function of the crystallinity of the substrate and the etching chemistry. The shape of the resulting microstructures becomes a convolution between the etch–mask pattern and the etching directionality. Hence, the narrow deep microstructures generally pursued in bulk micromachining are difficult to achieve, and better results are often achieved with the RIE techniques discussed above. A common RIE-based bulk-micromachining technique is the single-crystal reactive etching and metallization (SCREAM) process, which has been used to make deep microstructures in silicon and GaAs [3], [4]. The SCREAM process can produce structures having aspect ratios up to 50 or more (aspect ratio = maximum vertical feature/minimum lateral feature), and which span over lateral dimensions of 5 mm or more.

III. Overview of RF MEMS Components

Although it is still early for a time-tested categorization of RF-MEMS devices, the development to date tends to place them into different classes depending on whether one takes an RF or MEMS viewpoint. From the RF viewpoint, the MEMS devices are simply classified by the RF-circuit component they are contained in, be it reactive elements, switches, filters, or something else. From the MEMS viewpoint, there are three distinct classes depending on where and how the MEMS actuation is carried out relative to the RF circuit. The three classes are: 1) the MEMS structure is located outside the RF circuit, but actuates or controls other devices (usually micromechanical ones) in the circuit; 2) the MEMS structure

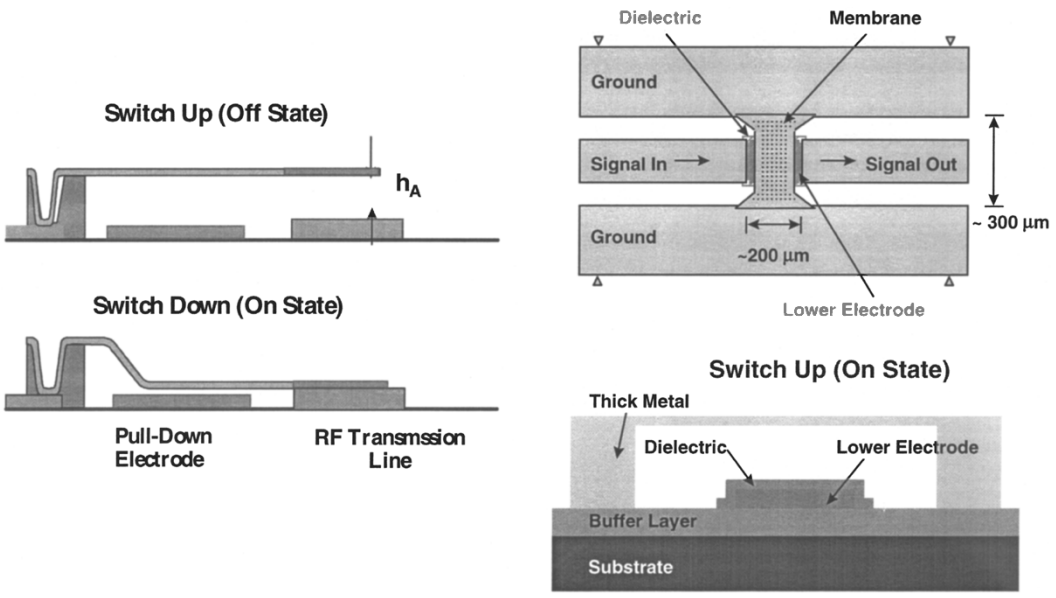

Fig. 2. Functional diagrams of two common RF MEMS switch structures. (a) Cantilever. (b) Air bridge.

is located inside the RF circuit and has the dual, but decoupled, roles of actuation and RF-circuit function; and 3) the MEMS structure is located inside the circuit where it has an RF function that is coupled to the actuation. We refer to each of these classes as: 1) RF extrinsic; 2) RF intrinsic; and 3) RF reactive.

Each of the MEMS classes has produced compelling examples, e.g., the tunable micromachined transmission line in the RF-extrinsic class, shunt electrostatic microswitch and comb capacitors in the RF-intrinsic class, and capacitively coupled micromechanical resonator in the RF-reactive class. A collection of these devices is shown in the RF MEMS technology diagram of Fig. 1. The richest class is clearly the RF-intrinsic, which already boasts three promising devices. Here, we have tunable capacitors and inductors that are expected to operate up to at least a few gigahertz in frequency, and we have RF-embedded switches that operate well from a few gigahertz up to at least 100 GHz.

This paper primarily concentrates on the switches, which are the essential devices for RF reconfigurability. In so doing, it will become apparent that the mapping between RF device and MEMS class is not unique. In other words, the switching function, or any RF function for that matter, can often be achieved by different MEMS configurations. This is one reason why RF MEMS have recently become interesting to many RF component and circuit engineers. Of course, another reason is the potential systems impact. Probably not since the advent of GaAs microwave IC's has an RF technology shown so much promise to improve system performance and affordability *at the same time*.

IV. RF MEMS Switches

The microswitch is arguably the paradigm RF-MEMS device. In essence, it is a miniaturized version of the venerable toggle switch. In addition to the three classes based on MEMS actuation, the switches can be categorized by the following three characteristics:

1) RF circuit configuration;
2) mechanical structure;
3) form of contact.

The two common circuit configurations are single pole single throw (SPST): series or parallel connected. The most common mechanical structures are the cantilever and the air bridge, shown schematically in Fig. 2(a) and (b), respectively. The common contact forms are the capacitive (metal–insulator–metal) and resistive (metal-to-metal). Each type of switch has certain advantages in performance or manufacturability that are addressed later in this paper.

As in all RF switches, definitions of actuation and metrics are necessary to characterize performance. Following electrical convention, the number of poles is the number of input terminals or ports to the switch, while the number of throws is the number of output terminals or ports. Any switch is assumed to be binary and digital in the sense that it can lie in one of only two possible actuation states. In the "on" state, the switch is configured to connect the input port to the output port, while in the "off" state, it is configured to disconnect the two ports. The conventional RF metrics are [5]: 1) insertion loss in the on state; 2) the isolation (i.e., $1/|S_{21}|$) in the off state; and 3) the return loss (i.e., $1/|S_{11}|$) in both states. While pedestrian to RF engineers, these definitions and metrics are helpful when analyzing some of the unique switch types that MEMS enable.

A. Mechanical Structures and Actuation

The cantilever consists of a thin strip of metal and dielectric that is fixed on one end and suspended over free space elsewhere. The bridge is a thin strip of metal and dielectric that is fixed at both ends and suspended over free space in the middle. The diaphragm is a thin membrane of metal and dielectric fixed around its periphery and suspended over free

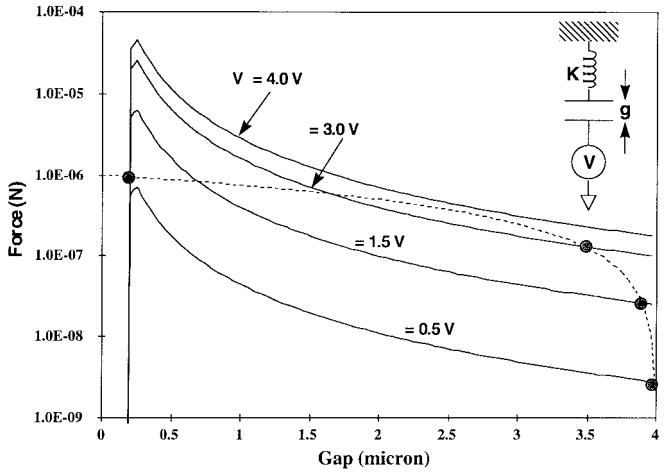

Fig. 3. Plot of equilibrium forces versus the gap dimension in a typical bridge switch. The inset shows the equivalent mechanical model for the bridge switch.

space in the middle. Some or all of the metallic parts of the cantilever, bridge, or diaphragm is suspended over a bottom metal contact in such a way that the two contacts form a capacitor. When a bias voltage is applied between the contacts, charge distributes in such a way that an electrostatic force occurs between them. Independent of the voltage polarity, the voltage forces the top contact down toward the bottom one, creating an opposing tensile force as the structure is bent. When the applied voltage reaches a certain threshold value $V_{\rm th}$, the tensile force can no longer balance in detail the electrostatic force, and the cantilever abruptly falls to the bottom contact. If the magnitude of voltage is then reduced, the cantilever releases back up, but typically at a much lower voltage than $V_{\rm th}$. This creates a hysteretic characteristic (typical of all MEMS switches).

The actuation behavior of electrostatic MEMS switches can be understood from the equivalent parallel-plate capacitor shown in the inset of Fig. 3. The bottom plate is fixed in space and the top plate is held by a spring having constant K. With an applied voltage V, the force on the top plate is given by $F = \varepsilon_0 A V^2/2g^2$, where ε_0 is the permittivity of free space, A is the effective area of the capacitor, and g is the physical separation between the contacts (i.e., the gap). Of course, this force is counteracted by a strong repulsive force when the plates touch, which arises from solid-state compression in the material making up the plates. This force can be approximated by the $f\theta(-g)$ where f is a (large) force constant and θ is the unit step function. Assuming that the spring behavior follows Hooke's law, the upward force on the top plate is given by $K(g_0 - g)$ where g_0 is the relaxed gap. For an arbitrarily applied voltage, the gap is found by balancing the two counteracting forces $\varepsilon_0 A V^2/2g^2 - f\theta(-g) - K(g_0 - g) = 0$.

A good example of actuation in RF-MEMS switches occurs in the air-bridge (or double-clamped beam) structure. In this case, the equivalent-spring constant is approximately by $K = 16Y \cdot W(T/L)^3$, where Y is Young's modulus, and W, T, and L are air-bridge width, thickness, and length, respectively. Typical values of these quantities in actual switches are $W = 100$ μm, $T = 0.5$ μm, $L = 400$ μm, and $Y = 8 \times 10^{10}$ N/m^2 (gold), so that $A = 4 \times 10^4$ μm^2 and $K = 0.25$ N/m. The typical relaxed gap dimension is 4 μm and it is assumed that there is a 0.2-μm layer of Si_3N_4 on top of the bottom electrode. Substituting these values into the force–balance expression, one can determine the equilibrium gap graphically by plotting the forces versus the gap dimension, as shown in Fig. 3. The dashed curves represent the spring force, and the solid lines, parametrized by different bias voltages, represent the sum of the electrostatic and compression forces. The solid curves display a concave-up region over the major range of gap dimension where the force is primarily electrostatic, and a precipitous drop down to the gap dimension equal to the bottom dielectric layer.

The intersection between the curves in Fig. 3 represents the equilibrium solution. By increasing the voltage gradually from 0.0 to 0.5, 1.5, and 3.0 V, one can see the gap slowly decrease from 4 to 3.45 μm. By 4.0 V, there is no longer an intersection between the curves over the electrostatic range, and the only possible solution is the intersection in the compressive range where the gap is at 0.2 μm and the force is approximately 1×10^6 N. Upon decreasing the voltage back through the same increments, this intersection persists (i.e., the air bridge remains pinned to the bottom dielectric) until the voltage drops to just above 0.5 V. At this point, the only possible intersection is back in the electrostatic region at a gap just below 4.0 μm. The resulting behavior of gap dimension (or capacitance) versus voltage is very hysteretic, similar in many ways to the behavior of output voltage versus input voltage in electronic latches.

The above analysis is helpful for physical insight, but ignores some practical effects that can affect the actuation values in real switches. Two such effects are stress in the air-bridge material comprising the top contact, and "stiction" between the bridge and bottom contact. For metal air bridges, the stress is generally tensile and often occurs at levels exceeding 10^7 Pa. This has the effect of increasing the spring constant (i.e., moving up the dashed curve in Fig. 3), so that the threshold voltage for switching is increased substantially. Stiction describes the process whereby the top and bottom electrodes bond together by microscopic surface forces. It is a strong function of the surface morphology of the contacts, and is particularly problematic in metal-to-metal switches. The addition of a thin dielectric layer between the metals, such as that described in the above analysis, helps mitigate this problem.

Due to the capacitive nature of the actuation, all of the RF MEM switches do not require continuous dc current for operation. In this sense, the control of these switches is like the control of CMOS switches. Associated with the control electrodes in the MEMS switch is a capacitance in the on and off states, $C_{\rm on}$ and $C_{\rm off}$, respectively. The electrostatic energy required to put the switch into one of these states is just $(1/2)CV^2$. Independent of the type of switch, the switch state with control electrode drawn down will dominate in both capacitance and voltage. Hence, the power dissipated is approximately $P_S \sim (1/2)CV^2 f_S$, where f_S is the switching rate. For example, the air-bridge device simulated and analyzed above has a switch-down capacitance

of 13 pF, so that if we assume a down-state bias voltage of 4 V and a switching frequency of 10 kHz, the power dissipation is approximately 1 μW.

Due to the low power dissipation and bias current, the RF isolation in the bias circuit of MEMS switches is relatively simple and can be carried out with resistors. In contrast, the much larger dc current drawn by traditional solid-state RF switches forces the isolation to be carried out with inductors because resistors would create too much voltage drop. In general, IC resistors are much smaller and cheaper than inductors and can be fabricated monolithically when the RF MEMS switch is fabricated on silicon.

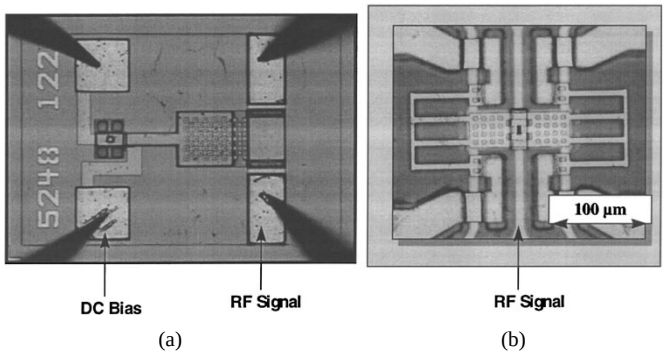

Fig. 4. Micrographs of the SPST switches developed at (a) Hughes Research Laboratories and (b) Rockwell Science Center.

B. Dynamic Characteristics

Additional issues in MEMS switches are their dynamic response and their switching time. To first order, the dynamic response can be estimated from the equivalent-spring model in the absence of electrostatic or compressive forces, which predicts a natural resonance frequency given by $f = (K/M)^{1/2}/2\pi$. From the parameters derived above and the density of the air bridge, the natural resonance is found to be 25.4 kHz, which is a typical value found on experimental MEMS switches. The switching time is more difficult to predict because it pertains to the time required for the air bridge to drop from threshold state to the bottom contact under the effect of electrostatic force. Since this force increases as the gap closes (as $1/g^2$), the switch-down time is substantially shorter than one might first guess. Typically, structures having the size and characteristics of the air bridge analyzed above will switch from the up to down state in roughly 1 μs. In contrast, switching from the down state to up state is much slower, taking roughly 10 μs. It is this longer time that is usually quoted as the limitation of RF-MEMS switching speed. Switch types other than air bridges may help ease this limitation and are currently being pursued by the MEMS device community.

When an ac voltage is applied to the microswitch at frequencies much less than the natural frequency, the membrane follows the ac waveform with nearly the same response as at dc. Hence, the ac waveform will induce switching when its amplitude exceeds the threshold voltage. At frequencies much greater than the natural frequency, the membrane no longer follows the instantaneous waveform and, instead, responds only to the root mean square (rms) voltage between the electrodes. This makes the MEMS switch very linear with respect to the high-frequency signal. In other words, when signals at two different frequencies are incident on the switch through the RF line, there is practically no mixing or intermodulation between the two signals. This is quite unlike the case in solid-state switches (e.g., p-i-n diodes or FET's) where the inherent nonlinearity of the current–voltage curves of the device makes intermodulation much stronger and problematic at power levels as low as 100 mW.

In spite of their inherent superiority in linearity, most if not all, of the RF-MEMS devices have displayed RF-induced switching. This occurs roughly when the rms voltage becomes large enough to close the switch by itself with no assistance from the dc bias. The corresponding RF power level depends on the switch type and its physical characteristics. The exact reason for this is currently being investigated by RF-MEMS researchers.

C. Switch Examples

To date, several RF-MEMS switches have been developed and tested, but two types stand out because of their continued pursuit by several different organizations: 1) the RF-extrinsic, cantilever- or spring-actuated switch having a metal beam on the free end of the cantilever that forms an SPST series-configured metal-to-metal contact and 2) the RF-intrinsic self-actuated bridge switch that forms an SPST parallel-configured metal–insulator–metal contact. Structures other than cantilevers and bridges (e.g., diaphragms) have also been investigated, but their performance has been inferior for one reason or another. There are currently also some single-pole multithrow switches under investigation, but no conclusive results have been reported so far. Thus, in this paper, only the cantilever-actuated series-configured beam and self-actuated parallel-configured bridge will be discussed further.

1) RF-Extrinsic Series-Configured Switch: Shown in Fig. 4(a) and (b) are micrographs of the SPST switches developed at Hughes Research Laboratories (HRL), Malibu, CA, and the Rockwell Science Center, Thousand Oaks, CA [6], respectively. In both cases, the RF contact is established by a metal beam that in the switch-on or down state establishes continuity by bridging the gap in an RF transmission line. In the HRL switch, the metal beam is mounted on one end of a single dielectric cantilever with a metal pad at its center. Electrostatic force between the pad and a bottom electrode actuate the switch. In the Rockwell switch, the metal beam is mounted in the middle of a dielectric folded spring, which is also actuated by a metal pad within its extent. In both cases, there is a large actuation structure designed for high leverage and relatively long physical throw. This allows for significant force to be applied to the metal-to-metal RF contact in the on state, and for a significant gap (many microns) to be created between the metal contacts in the off state. The result is low insertion loss and high isolation.

Shown in Fig. 5 are the experimental results for the metal-to-metal switches. Qualitatively, the RF characteristics of both

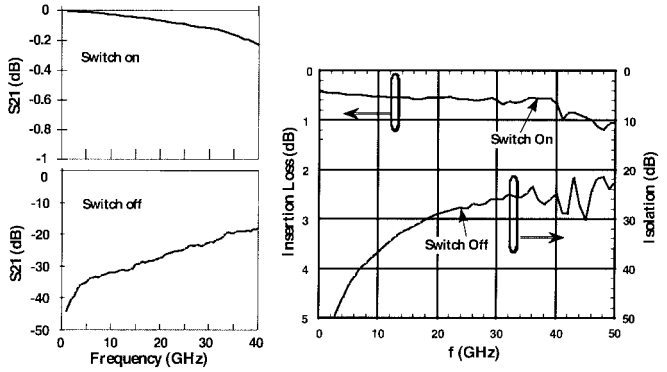

(a) (b)

Fig. 5. Experimental results for the metal-to-metal switches. (a) Transmission parameter for HRL switch in on state (upper) and off state. (b) Insertion loss and isolation of Rockwell Science Center switch in on state and off state, respectively.

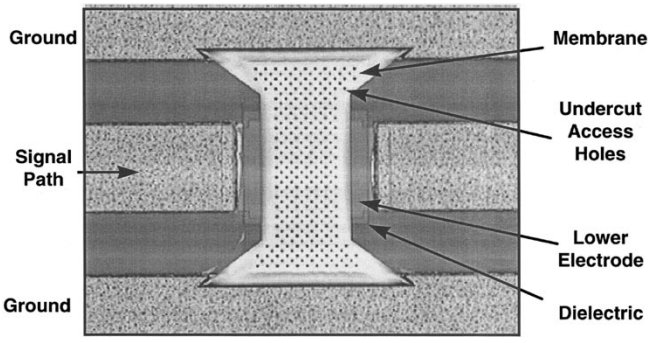

Fig. 6. Micrograph of the SPST parallel-configured air-bridge switch developed at Texas Instruments (now Raytheon/TI).

switches are similar. In the HRL switch of Fig. 5(a), the insertion loss (upper graph) increases very gradually with frequency from less than 0.1 dB below 1 GHz to approximately 0.25 dB at 40 GHz. In the Rockwell switch of Fig. 5(b), the insertion loss increases from about 0.4 dB below 1 GHz to just over 1 dB at 40 GHz. The isolation for the HRL switch (lower graph) degrades from about 40 dB below 1 GHz to about 20 dB at 40 GHz. The Rockwell switch is superior in isolation, ranging between better than 50 dB below 1 GHz to approximately 25 dB at 40 GHz. The superiority in isolation of the Rockwell switch is attributed in part to its greater vertical displacement.

2) RF-Intrinsic Parallel-Configured Switch: Shown in Fig. 6 is a micrograph of the SPST parallel-configured bridge switch developed at Texas Instruments Incorporated (now Raytheon/TI), Dallas, TX. The RF contact is established by a metal–insulator–metal bridge that, in the switch down or off state, loads the center conductor of an RF transmission line with a small capacitive reactance to the ground plane. Electrostatic force between the top and bottom electrodes actuates the switch. Unlike the series-configured switches, the actuation structure for parallel-configured bridges is the same as the switching structure. The insertion loss and isolation are related to the capacitance of the switch in its on and off states. For low insertion loss, the "on" capacitance (switch up) $C_{\rm on}$ should be as low as possible, and for high isolation, the "off" capacitance $C_{\rm off}$ (switch down) should be as high as possible. Hence, a useful figure-of-merit is the ratio $C_{\rm off}/C_{\rm on}$.

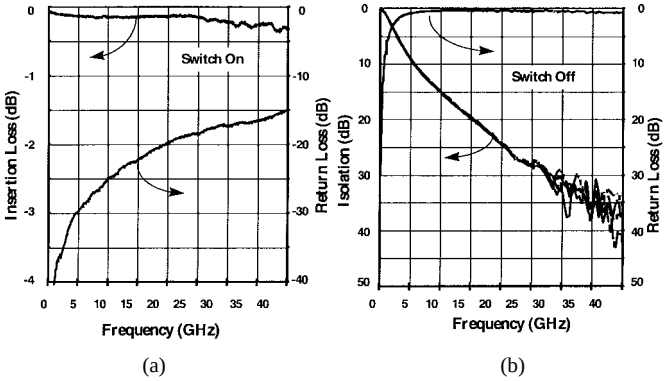

(a) (b)

Fig. 7. Experimental results for the Raytheon/TI metal–insulator–metal switch in (a) the on state and (b) off state.

In the parallel-plate approximation $C_{\rm on} = [h_A/\varepsilon_0 A + h_D/\varepsilon_D A]^{-1}$ and $C_{\rm off} = \varepsilon_D A/h_D$, where h_A is the thickness of the air gap, h_D is the thickness of the insulating layer, ε_D is the dielectric constant of the insulating layer, and A is the effective area of the capacitor. Hence, the ratio is given by $C_{\rm off}/C_{\rm on} = 1 + \varepsilon_D h_A/\varepsilon_0 h_D$, independent of area. As an example, the air gap in the switches of Fig. 6 is typically 2 μm, the insulator thickness is approximately 0.1 μm, and its dielectric constant is typically 7.5. This yields an on-to-off ratio of 151. In contrast, the ratio $C_{\rm on}/C_{\rm off}$ in a typical solid-state varactor switch, such as a reverse-biased Schottky diode, is limited to values around ten or less. This is because the capacitance is determined mostly by the length of the depletion region, which, to first order, varies as the square root of the reverse voltage. Also, the reverse bias must be limited to levels of roughly tens of volts to avoid the reverse-breakdown mechanisms.

Shown in Fig. 7 are the experimental results for the metal–insulator–metal switch. The insertion loss in Fig. 7(a) is similar qualitatively to that of the metal-to-metal switches, increasing gradually with frequency between approximately 0.1 dB below 1 GHz to about 0.3 dB at 40 GHz. The high-frequency values are remarkably close to those in Fig. 5(a) for the metal-to-metal switch. In contrast, the isolation behavior in Fig. 7(b) differs from that of the metal-to-metal switch substantially. Quantitatively, the isolation of the metal–insulator–metal switch is rather poor at low frequencies, being approximately 0 dB at 1 GHz. Also, opposite to the metal-to-metal switch, the isolation improves with frequency, approaching values around 35 dB at 40 GHz. The explanation for these results stems largely from the fundamental difference in electrical behavior between a series and parallel switch, as discussed further in Section IV-D.

This same switch has also been characterized for linearity and power-handling capability. In experiments conducted between 2–4 GHz, no intermodulation spurs were observed with signal powers ranging up to 20 dBm [7]. Hence, only a lower limit could be established on the third-order intermodulation product (IP3), where IP3$>+66$ dBm. In experiments to assess the power-handling capability, similar switches were observed

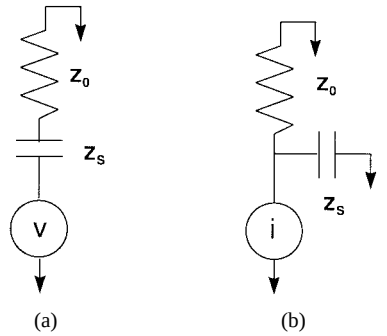

Fig. 8. Equivalent circuit diagrams for (a) series configured MEMS switch and (b) parallel-configured MEMS switch. In these circuits, Z_S is the impedance of the switch in the off state and Z_0 is the characteristic impedance of the transmission line in which the switch is embedded.

to self-close with approximately 3-W CW power at 10 GHz and with approximately 1 W CW at 35 GHz [8].

D. Comparison of Series and Parallel Switches

The marked difference in isolation between the series and parallel MEMS switch configurations can be explained qualitatively, at least at low frequencies, by the equivalent circuits of Fig. 8. In these circuits, Z_S is the impedance of the switch in the off state and Z_0 is the characteristic impedance of the transmission line in which the switch is embedded. For both configurations, $Z_S \sim 1/j\omega C_S$ in the off state where C_S is relatively small in the series switch and large in the parallel switch. By definition, the isolation I is the power from the source divided by the power delivered to the load or $I = 1/|S_{21}|$ where S_{21} is the forward-scattering parameter. For the series model of Fig. 8(a), circuit analysis yields $I = (\omega Z_0 C_S)^2/[1+(\omega Z_0 C_S)^2]$. For the parallel switch of Fig. 8(b), $I = 1/[1 + (\omega Z_0 C_S)^2]$. Both expressions are consistent with the observed low-frequency behavior. The isolation of the series switch approaches zero (i.e., $-\infty$ dB) in the limit of zero frequency and degrades with frequency as ω^2. The isolation of the parallel switch approaches unity (i.e., 0 dB) in the limit of zero frequency and remains relatively constant up to a rolloff frequency of $f \sim 1/(2\pi Z_0 C_S)$. Well above this frequency, the isolation improves with frequency as ω^{-2}.

As an example, we consider the parallel-switch configuration made with the typical air-bridge analyzed earlier having an area of 4×10^4 μm^2, a dielectric thickness of 0.2 μm, and a dielectric constant of 7.5. This leads to an off capacitance of $C_S = 13.3$ pF. If we assume the typical characteristic load impedance of $Z_0 = 50\ \Omega$, the rolloff frequency is found to be 240 MHz. This explains why the isolation in Fig. 8 is increasing approximately as ω^{-2} starting at the lowest frequencies of the plot.

The equivalent-circuit model is not expected to predict the high-frequency behavior of the switches because it ignores the effect of surface modes. All planar transmission lines on dielectric substrates are known to harbor these modes, the number of which generally increases with frequency. The surface modes can bypass the discontinuity created by the off-state switch such as the gap in the center conductor of a series switch or the shunt between the center conductor and the ground plane created from a parallel switch. In so doing, the surface mode couples to the opposite side of the transmission line with an efficiency that depends on many factors, such as the spatial form of the mode. Although detailed analysis is pending, some RF-MEMS researchers believe that surface-mode coupling will ultimately limit the isolation of series and parallel RF MEMS switches to values in the range of 40–50 dB.

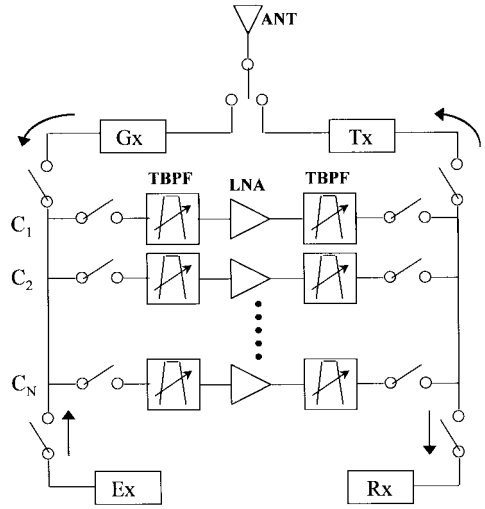

Fig. 9. Typical VHF and UHF switchable radio front-end that must operate simultaneously with other RF transmitters at the same physical site.

V. Circuit Applications

A. Signal Routing in RF System Front-Ends

The low insertion loss and high isolation of the metal-to-metal microswitches across the common RF bands combined with their low bias power and physical compactness makes them attractive for the function of RF routing in the front-end of many systems. A good example is the radio front-end, as shown in the block diagram of Fig. 9. This is a type of radio that must operate simultaneously with other RF transmitters at the same physical site. In this case, there is a strong tendency for "cosite" interference, which requires very high dynamic-range receivers, very clean transmitters, and careful attention to the overall electromagnetic compatibility. This generally requires filters on each transmitter (Tx) and receiver (Rx) to ensure that cross interference or signal jamming is minimized. The filters must have a narrow instantaneous passbandwidth, high rejection out-of-band, widely tunability, and low insertion loss.

Due to the great difficulty, if not impossibility, in achieving all of these filter characteristics simultaneously over many radio channels, the practical solution is to decompose the filtering task. The entire spectrum to be covered by the radio is divided into several independent channels ($C1, C2, \cdots, CN$ in Fig. 9), each of which has a filter of achievable instantaneous bandwidth, rejection, tunability, and insertion loss. RF switches are then required at the input of each channel to connect to the antenna or the exciter depending on whether

the radio is receiving or transmitting. Simultaneously, switches at the output of each channel must connect the output to the receiver or transmitter electronics. Altogether, the network of switches and filters shown in Fig. 9, which is called a frequency preselector, is often very massive, power consuming, and expensive.

A good example of such a front-end is the ARC-210, probably the premier radio today for military airborne communications in the VHF and UHF bands between 30–400 MHz. It comprises five independent channels at: 1) 30–88 MHz; 2) 108–136 MHz; 3) 136–156 MHz; 4) 156–174 MHz; and 5) 225–400 MHz, four of which can be scanned. Among other characteristics, it has a front-end noise figure of 4.5 dB, a 1-dB-output compression of +14 dBm (receive) and +9 dBm (transmit), and a 75-μs tuning time over 160-kHz steps. Most of the RF switching in the ARC-210 is done by 27 p-i-n diodes, each of which consumes many milliwatts of power and provides less-than-desirable isolation. The superior isolation of the MEMS switches (in combination) should improve the transmit/receive isolation from 60 to >80 dB, with commensurate reduction in intermodulation distortion. The lower insertion loss of the MEMS should reduce the front-end noise figure from 4.5 to 4.0 dB. Also, the lower power dissipation of the MEMS should reduce the total power consumption from roughly 100 mW to less than 1 mW.

While the ARC-210 is now considered a legacy system, the frequency preselector architecture is rather generic and could apply to a variety of future radio and wireless systems, For example, it is believed that the wireless transceiver of the future will need to access a number of bands, including 0.9- and 2.1-GHz PCS, 5.3-GHz Supernet, and perhaps others. It will also have to do so in an environment of increasing cosite and other forms of EMI. The MEMS switches in the preselector will easily scale with frequency, as implied by the experimental data given above for the example switches. A related question is the stability of the tunable filters, which is being addressed by the development of high quality (Q) tunable MEMS filters. The most promising one for the PCS bands and higher is presently the MEMS *LC* tank filter in which both the inductor and capacitor are made by surface micromachining techniques. To read more about this fascinating filter technology, the reader is referred to [9].

B. Digitized Capacitor Banks

As explained above, the development of RF-embedded MEMS switches affords new circuit applications not practical with RF-separated devices. An excellent example is the use of MEMS switches in digital capacitor banks. This is a promising way to get a variable capacitance (although not with continuous variability) that is highly linear and has high Q factor up to microwave frequencies. Existing semiconductor devices can provide continuous tunability (e.g., back-biased Schottky diodes) of capacitance up to very high frequencies well into the millimeter-wave band and beyond. However, their intrinsic Q factor $Q \sim \omega C/G$ is limited to fairly low values because of the significant conductance G in semiconductor devices. This arises in Schottky diodes, for example, by reverse leakage through the depletion layer, and generally limits the Q to values less than ten. It is interesting that even Si nMOS varactors display Q values in this range [10].

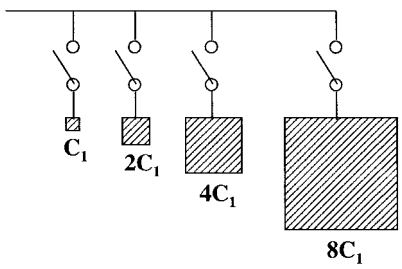

Fig. 10. A 4-b capacitance bank containing fixed-value thin-film capacitors connected to external circuit through MEMS switches.

The MEM switches can be used to make high-frequency high-Q capacitors in several different ways using both the RF-separated and RF-embedded devices. The first indication of this capability was reported in 1996 using a diaphragm variable capacitor having a Q of 62 at 1 GHz [11]. Fig. 10 shows the schematic diagram of a binary capacitor bank made by using the air-bridge metal–insulator–metal structure as a capacitance bit. This is made possible by the fact that the ratio of unactuated (bridge up) to actuated (bridge down) capacitance is so large (typically >100) in this structure. A multibit capacitance bank is then formed by fabricating other structures with a binary relationship in the area, and connecting them in parallel, as shown schematically in Fig. 10. Using such a technique, a research and development team developing such capacitor banks for tunable filters has fabricated a 6-b bank having a range of capacitance between 0.5–32 pF. Q measurements are currently pending.

B. Phase-Shifting Networks

1) Discrete- and Analog-Tuned Time-Delay Lines: One of the more ubiquitous control functions at microwave and millimeter-wave frequencies is phase shifting. For example, it is essential to the operation of phase-lock loops and phased-array antennas in receivers and transmitters alike. MEMS switches benefit RF phase-shifting technology in a number of ways, not the least of which is the ability to realize some phase-shifter circuits that, while promising in principle, have not been very successful because of performance limitations with traditional solid-state technology. One such circuit is shown in Fig. 11. It is a time-delay phase shifter in which N (three, in this case) different binary loops are connected in series to provide 2^N possible electrical delays between the input and output ports. Each loop has two arms of different electrical length, and contains switches to force the RF signal down one or the other of the arms. By choosing the length of each loop appropriately, the 2^N electrical delays are equal to an integral multiple of the least significant delay plus a built-in offset delay. This creates a digital phase-shifter function.

As in many phase-shifter designs, it is desirable to have the maximum phase shift (maximum electrical length) equal to $2\pi(\lambda)$, so that the least-significant phase shift becomes $2\pi/2^N(\lambda/2^N)$. As an example, we consider the case of Fig. 11, where $N = 3$ and the least-significant phase shift

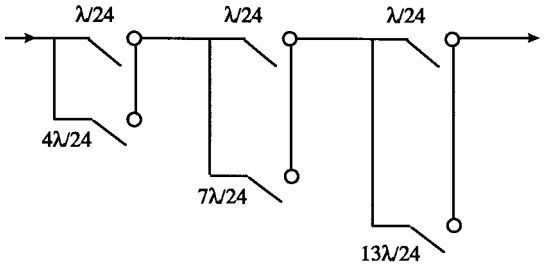

Fig. 11. Schematic diagram of time-delay phase shifter in which N (three, in this case) different binary loops are connected in series to provide 2^N possible electrical delays between the input and output ports.

(delay) is $2\pi/8(\lambda/8)$. Ignoring the built-in phase-shift offset arising from the length of lines connecting the loops, we can write the digital phase shift or time-delay characteristic for this circuit as $\phi_n = 2\pi n/8$ or $t_n = v^{-1}n\lambda/8$, respectively, where $n = 1, \cdots 8$, and v is the phase velocity on the lines. While simple to control and intrinsically wide-band, the digital time-delay phase shifter can be too coarse for some applications since the phase accuracy is inherently limited to the least-significant bit. This can be overcome only by adding more bits (loops) in the circuit, which has the adverse affect of adding propagation losses and circuit area. A compromise in many RF-sensor (e.g., radar) applications is 4-b (22.5° phase accuracy).

A clever means of achieving time-delay phase shifting while reducing the circuit area and improving the phase accuracy has been demonstrated recently at the University of Michigan at Ann Arbor [12]. The approach is a coplanar-waveguide transmission line periodically loaded with MEMS switches. Each switch is fabricated in the parallel configuration directly across the line in such a way that a variation in the gap of the parallel switches changes the capacitance and, hence, the phase shift and electrical time delay down the line. The phase shift is $\phi = \omega t_d$ where the time delay is given by $t_d = \Lambda/v = (\Lambda)[L'(C' + C_S/p)]^{1/2}$. Here, Λ is the physical length of line, C' and L' are the specific capacitance and inductance, respectively, of the unloaded line, and p is the physical period of the MEMS bridges. Analog control is provided by electrostatic control of Cs, which generally only provides about 33% variation of the relaxed capacitance before pull down occurs. Although a single switch is thus a relatively limited analog varactor, the combined effect of many switches on the loaded transmission line is substantial. For example, a 10.1-mm-long loaded line has been fabricated with 32 MEMS air-bridges having 30-μm width and 306-μm period. The result was a nearly linear dependence of phase shift on frequency from dc up to 60 GHz with a slope that depended smoothly on switch bias voltage. The value of slope was approximately 0.3°/GHz at 10-V bias, 0.7°/GHz at 15-V bias, 1.3°/GHz at 20-V bias, and 1.7°/GHz at 22-V bias. Remarkably, the insertion loss was not too much higher than that of the unloaded line, being 1.8 dB at 40 GHz, 2.0 dB at 60 GHz, and largely independent of bias voltage.

1) Incorporation Into Phased Arrays: The importance of time-delay phase shifting is made evident in Fig. 12(a) and (b), where the signal at frequency ω_1 from two antenna elements

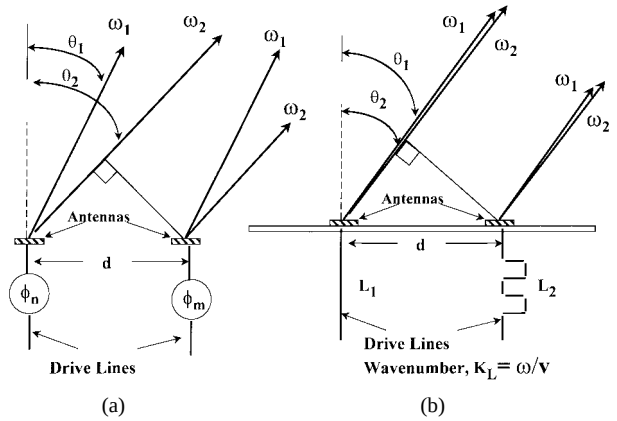

Fig. 12. Schematic diagram of electromagnetic interference between two adjacent antenna elements driven by (a) conventional phase shifters and (b) time-delay phase shifters.

separated by distance d is passed through conventional phase shifters and a time-delay network, respectively. In both cases, the antennas will interfere constructively at an angle θ_1 (relative to the zenith) where the difference in phase shift feeding the elements $\Delta\phi$ matches the difference in phase incurred through the radiation along angle θ_1, which is given by $(\omega_1 d/c)\sin\theta_1$. This expression leads to constructive interference at the angle $\theta_1 = \sin^{-1}[c\Delta\phi/\omega_1 d]$.

For a conventional phase shifter, $\Delta\phi$ is independent of frequency to first order. Hence, if a second signal at frequency ω_2 is passed through the phase shifters, the constructive interference will occur at a different angle of $\theta_2 = \sin^{-1}[c\Delta\phi/\omega_2 d]$. For time-delay phase shifting, $\Delta\phi$ depends on frequency as $\Delta\phi = k(L_2 - L_1) = \omega(L_2 - L_1)/v$ where L and v are the physical length and the velocity of radiation, respectively, for the delay line. Substitution of this into the constructive-interference condition yields $\theta = \sin^{-1}[c(L_2 - L_1)/vd]$, which is independent of frequency.

The variation in constructive-interference angle with frequency is called "squint" and has long been known as a problem in constructing RF phased arrays having wide instantaneous bandwidth. By the same token, time-delay phase shifters have long been sought as a solution to this problem. Traditional solid-state switches such as p-i-n diodes and FET's introduce cost, performance, or bias-power problems in the typical arrays used for radar and communications (thousands of antenna elements). P-i-n diodes have low insertion loss, but consume great bias power and are not readily integrated with their bias and other RF electronics. Although much more integrable, FET's have higher insertion loss because they are not very good resistive (on/off) switches. At microwave frequencies, the finite on-resistance typically leads to an insertion loss of 1 dB (i.e., 21%) and, because at least one switch is required for each bit in the time-delay phase shifter, at least half of the transmit power is lost to the switches alone, not accounting for transmission-line and other losses.

RF-MEMS switches are promising because they can simultaneously provide the RF performance (low insertion loss and high isolation) comparable to or better than p-i-n diodes, the circuit integrability of FET's, and a bias power consumption much less than either. Given the levels of switch performance

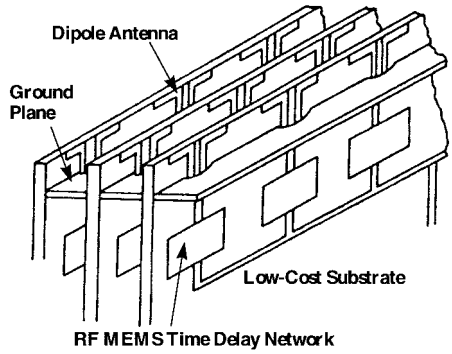

Fig. 13. Conventional "slat" phased-array architecture in which the phase shifters and other RF electronics are integrated with planar antennas on parallel cards.

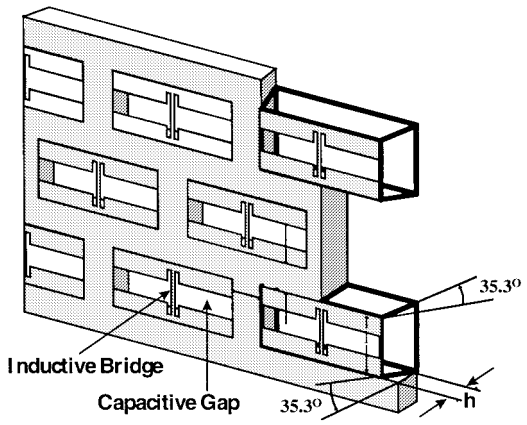

Fig. 14. Quasi-optical beam-steering component made by MEMS switches across waveguides micromachined into silicon substrates.

plotted in Fig. 7, it has been projected that 4-b phase shifters will be realized that have roughly 2.5 dB of total insertion loss in X-band (centered at 10 GHz) and 3.5 dB of total insertion loss in Ka-band (centered at 35 GHz) [13]. More than 50% of these values arises from RF losses in the transmission line and MEMS bias lines. In principle, the losses in the lines could be reduced by bulk micromachining techniques such as those developed at The University of Michigan at Ann Arbor [14], [15].

A promising architecture for the insertion of MEMS phase shifters is the "brick" array, shown in Fig. 13, in which the phase shifters and other RF electronics are integrated with planar antennas on parallel slats [16]. Note that the relatively slow switching speed of the MEMS switches does not necessarily hinder the system performance in such arrays. For example, when used for beam steering in long-range radar or communications systems, the phase shifters are usually adjusted on time scales of microseconds or longer.

VI. The Future

A. Quasi-Optical Components

Quasi-optical techniques entail the processing and control of electromagnetic signals as they are propagating in free space or an extended spatial mode rather than in the confined transmission line of a microwave IC. In general, quasi-optical components consist of arrays of individual solid-state devices or monolithic microwave integrated circuits (MMIC's) in the region of space where the electromagnetic beam or mode passes through. These arrays operate on the entire beam or mode in a cooperative fashion under separate electronic control. Some of the processing functions that can be carried out are beam steering, power amplification, and frequency multiplication [17].

Although many good quasi-optical circuits have been studied to date, most of them have been hindered in performance or fabrication by the presence of the substrate material used to make the devices or MMIC's. Whether it is GaAs, Si, or some other high-speed semiconductor material, the high dielectric constant makes it difficult to couple radiation efficiently from free space (or an extended mode) to the substrate and then back out again. MEMS offers a solution to this problem in two key ways. The bulk micromachining can be used to remove the substrate where it causes problems in RF behavior, and the surface micromachining can be used to make switches and other device that offer performance characteristics far better than their semiconductor counterparts. Of course, this presupposes that the substrate used for the MEMS fabrication is amenable to bulk micromachining, so that silicon is usually favored.

A good example of a quasi-optical component made by MEMS switches and micromachining is the beam-steering array shown in Fig. 14, which is based on a concept developed in the early 1990's [18]. It consists of a triangular lattice of rectangular holes in a silicon substrate. The holes are created by bulk micromachining of silicon using a wet chemical etchant. The holes have sloped walls consistent with the anisotropy of wet etchants. Each hole is metallized to act like a waveguide, and the mouth of each hole is covered with a silicon oxynitride membrane on which RF circuit elements are fabricated. One element is a metal beam spanning across the narrow dimension of the rectangular waveguide and having a gap at its center. The next element is a MEMS (metal-to-metal) switch mounted across each gap.

Due to the low on-resistance of the MEMS switch, the metal beam across the waveguide is electrically continuous with the switch on (i.e., closed). In this state, the effect of the beam on the fundamental mode of the rectangular waveguide is a simple inductance. The value of the inductance is determined by the dimensions of the beam. This means that the phase of the electric field is advanced relative to having zero inductance. With the type of isolation demonstrated in the metal-to-metal switches earlier, the off (i.e., open) state of the MEMS switch should approach zero inductance.

To get more than 1 b of phase shift, multiple wafers can be stacked in the manner shown in Fig. 15. The number of wafers is chosen to achieve approximately a 2π difference in phase shift between all switches on and off. The substrates are separated by shims to achieve a precise electrical length between phase shifters. The edges of the silicon substrates are held in a flange that registers the substrates for alignment of the waveguides. An analysis of such a device has been carried out at 35 GHz, leading to the prediction of a steering angle of somewhat less than 40° (limited by the presence of grating

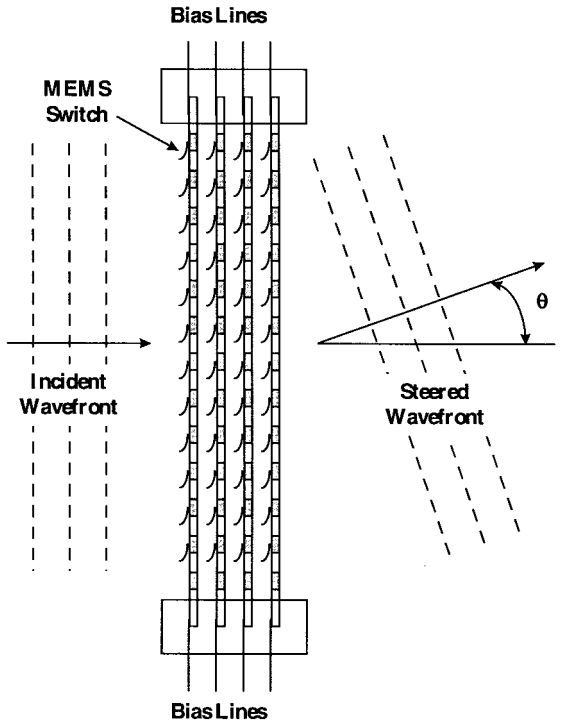

Fig. 15. Quasi-optical beam-steering wafers stacked in series to achieve multiple-bit phase control and nearly 2π overall phase shift.

lobes), approximately 3 dB of insertion loss and a 2-GHz operational bandwidth [19].

B. Reconfigurable Antenna Apertures

For several years, there has been considerable interest in developing antennas that can alter their radiating topology electronically. In a first step with this concept, one research group has been developing a planar dipole antenna containing a metal-to-metal MEMS series switch in each arm [20]. Since the switch is located approximately halfway between the driving gap and end of the arms, the resonant frequency is varied by about a factor of two between the switch-on and switch-off states. Assuming that the resonant impedance is nearly matched to the generator impedance at both frequencies, the switching action of the MEMS leads to high antenna gain at the two disparate frequencies, and it accomplishes this *within the same physical aperture*. This is quite distinct from another combination of switches and antennas popular in the wireless arena today. In the latter technology, known as "smart antennas," different antennas (i.e., different apertures) are judiciously connected to transceivers to achieve specific improvements in link performance and to mitigate the effects of multipath or cosite interference.

By implementing surface-micromachined MEMS switches over larger areas, it may be possible to extend the switchable antenna concept to form a fully reconfigurable aperture, as shown schematically in Fig. 16. This consists of a two-dimensional matrix of conducting "islands" separated by MEMS switches. By judiciously closing a subset of the switches and leaving the remainder open, one can, in principle, synthesize a large variety of conducting topologies ranging

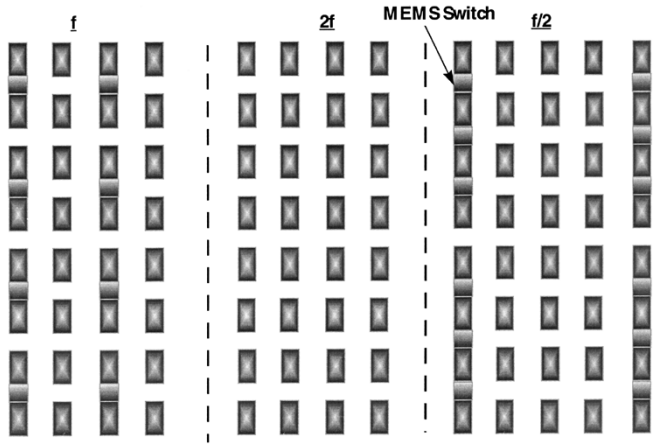

Fig. 16. Topological view of three configurations of an array of planar antenna elements made reconfigurable by MEMS switches that interconnect between the elements.

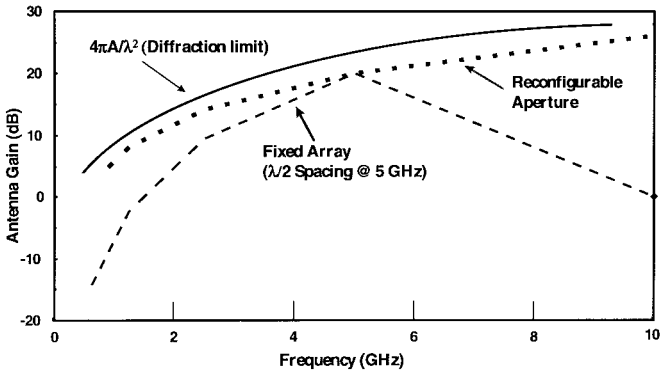

Fig. 17. Plot of theoretical antenna gain versus frequency for a 24 cm × 24 cm radiating aperture. 1) Diffraction-limited performance. 2) Approximate performance at 0.62, 1.25, 2.5, 5, and 10 GHz for a reconfigurable aperture in which the elements are changed to resonant length and half-wavelength separation at each frequency. 3) Approximate performance for fixed-element phased array designed for resonant length and half-wavelength element separation at 5 GHz.

from variable-spacing phased arrays, as shown in Fig. 16, to large single elements like an Archimedian spiral. In so doing, it should be possible to construct high-gain apertures that operate over much wider bandwidths than can be achieved today.

To understand the advantage of the reconfigurable aperture, it is helpful to look at the example of a phased array containing a square lattice of individual elements covering an area A. Suppose that each element is designed for impedance match to its generator at frequency f, is separated from its neighbors by approximately $\lambda/2 = c/2f$, and displays an elemental radiation efficiency of ε. Then according to the antenna theorem, the phased array as a whole should display a gain of $4\pi\varepsilon A/\lambda^2$. This point is quantified in the plot (labeled fixed array) of Fig. 17, where it is assumed that $f = 5$ GHz, $A = 24 \times 24$ cm, and $\varepsilon = 0.5$, so that $G = 19$ dB. For comparison, this plot also contains the diffraction-limited curve $G = 4\pi A/\lambda^2$ over the range of 0.5–10 GHz. For the given values, the diffraction-limited gain at 5 GHz is approximately 22 dB.

Now suppose that the frequency is increased twofold as in the middle part of Fig. 16. If the array configuration

remains the same as at 5 GHz, the aperture efficiency degrades substantially because of the onset of grating lobes near the horizon of the pattern. This is associated with a drop in the gain to roughly 0 dB. In contrast, if the aperture can reconfigure so that the element spacing is cut in half and the element length is reduced approximately two times, the gain will actually be 6 dB higher at 10 GHz than at 5 GHz, provided that the elemental radiative efficiency remains nearly constant. This result is shown in the reconfigurable aperture curve of Fig. 17, which is seen to track the diffraction-limited curve. Finally, when the frequency is decreased twofold to 2.5 GHz, the gain of the fixed array drops off again. This is because the elements now have less than the resonant length, the antenna impedance is much less than at 5 GHz, and a substantial fraction of the incident power is reflected back to the generator. In contrast, the reconfigurable aperture again remains within a few decibels of the diffraction-limited curve because, through switching, the elements are able to maintain the resonant length and impedance. At the same time, the separation between elements must increase approximately two times to accommodate the longer elements.

Clearly, the arguments just given depend on several assumptions regarding the reconfigurable aperture architecture. Firstly, it is assumed that every island in the switching matrix can be fed by transmit or receive electronics with the required values of amplitude and phase. This represents a significant challenge in RF routing and packaging, and may require the development of bulk micromachining transmission-line technology along the lines of that addressed in [9]. Secondly, it is assumed that the substrate on which the reconfigurable aperture is mounted represents no or little perturbation to the radiating elements, even over the multioctave bandwidths analyzed. To meet this assumption, the substrate may require an absorbing layer to prevent degenerative reflections from an otherwise reflecting back plane. This will certainly reduce the aperture efficiency. A better approach, but one requiring research and development, would be a passive or active back plane that could demonstrate zero phase shift to the electric field over octaves of bandwidth. While very challenging, it is conceivable that such a "zero phase shift" back plane could be created from the new class of artificial dielectrics (e.g., metallodielectric photonic crystals) or active frequency selective surfaces (e.g., reflect-array amplifiers).

C. Market Projection

Given acceptable development of design tools and manufacturing capability, it is expected that the market potential in RF MEMS will be substantial within the next 5–10 years. According to research conducted by Ernst & Young Entrepreneurs Conseil, Paris, France, in 1996, the MEMS market was $12 billion for devices and $34 billion for systems. The same firm estimates that by the year 2002, the market will have grown to $34 billion for devices and $96 billion for systems. The fraction of this market in RF MEMS is difficult to predict, but it is generally agreed that the RF portion along with a similar technology in optical devices and components are the most rapidly growing MEMS technologies today [21].

VII. Conclusion

In recent years, the field of MEMS has grown very fast and merged with many defense and commercial applications. Much of this activity has been driven by the ability of MEMS to miniaturize, reduce the cost, and improve the performance of, transducers and actuators previously fabricated by hybrid techniques. These benefits have stemmed from the compatibility of MEMS with silicon-based microelectronics and surface and bulk micromachining. This paper has dealt with a recent development along these lines called RF MEMS. Broadly speaking, RF MEMS is a new class of passive devices (e.g., switches) and circuit components (e.g., tunable transmission lines) composed of or controlled by MEMS. The most widely investigated RF MEMS device has been the electrostatic switch, consisting of either a thin metallic cantilever, air bridge, diaphragm, or some other structure that when pulled down to a bottom electrode shorts, opens, or loads an RF transmission line. Several applications of the switches were analyzed here, including switchable routing in RF system front-ends, digital capacitor banks, and time-delay networks. In the future, it is anticipated that RF MEMS will enable a new class of components and subsystems that are electrically reconfigurable. Two promising concepts discussed were discussed here: quasi-optical beam steering and reconfigurable antennas. In these and most applications being considered, RF-MEMS switches are promising a major positive impact on both performance and cost—a rare occurrence for any technology just entering the RF arena.

References

[1] A. Pisano, private communication.

[2] J. Bryzek, K. Petersen, and W. McCulley, "Micromachines on the march," *IEEE Spectrum Mag.*, p. 20, May 1994.

[3] K. A. Shaw, Z. L. Zhang, and N. C. MacDonald, *Sens. Acutators*, vol. 40, 1994.

[4] Z. L. Zhang and N. C. MacDonald, *J. Micromechanical Syst.*, vol. 2, pp. 66–72, 1993.

[5] K. Chang, *Handbook of Microwave and Optical Components*, vol. 1. New York: Wiley, 1989.

[6] J. J. Yao and M. F. Chang, "A surface micromachined miniature switch for telecommunications with signal frequencies from dc to 4 GHz," in *8th Int. Conf. Solid-State Sens. Actuators* Stockholm, Sweden, June 25, 1995, pp. 384–387.

[7] C. Goldsmith, J. Randall, S. Eshelman, T. H. Lin, D. Denniston, S. Chen, and B. Norvell, "Characteristics of micromachined switches at microwave frequencies," in *IEEE MTT-S Symp. Dig.*, San Francisco, CA, June 18–20, 1996, pp. 1141–1144.

[8] C. Goldsmith, private communication.

[9] C. T.-C Nguyen, L. P. B. Katehi, and G. M. Rebeiz, *Proc. IEEE*, vol. 86, pp. 1756–1768, 1998.

[10] M. Soyuer, K. A. Jenkins, J. N. Burghartz, and M. D. Hulvey, "A 3-V 4-GHz nMOS VCO with integrated resonator," in *IEEE Int. Solid-State Circuits Conf. Dig.*, San Francisco, CA, 1996, pp. 394–395.

[11] D. J. Young and B. Boser, "A micromachined variable capacitor for monolithic low-noise VCO's," in *Solid-State Sens. Actuator Workshop Tech. Dig.*, Hilton Head, SC, 1996, pp. 86–89.

[12] N. S. Barker and G. M. Rebeiz, "Distributed MEMS true-time delay phase shifters and wide-band switches," *IEEE Trans. Microwave Theory Tech.*, vol. 46, Apr. 1998.

[13] C. Goldsmith, Raytheon/TI Syst., private communication.

[14] L. P. B. Katehi and G. M. Rebeiz, "Novel micromachined approaches to MMIC's using low-parasitic, high-performance transmission media and environments," in *IEEE MTT-S Symp. Dig.*, vol. 2, San Francisco, CA, June 18–20, 1996, pp. 1145–1148.

[15] S. V. Robertson, L. P. B. Katehi, and G. M. Rebeiz, "A 10–50 GHz micromachined directional coupler," in *IEEE MTT-S Dig.*, vol. 2, San Francisco, CA, June 18–20, 1996, pp. 797–800.
[16] R. J. Mailloux, *Phased Array Antenna Handbook*. Norwood, MA: Artech House, 1994, sec. 5.3.
[17] R. A. York and Z. B. Popovic, *Active and Quasi-Optical Arrays for Solid-State Power Combining*. New York: Wiley, 1997.
[18] J.-C Chiao and D. B. Rutledge, "Microswitch beam-steering grid," in *Proc. Int. Conf. Millimeter Submillimeter Waves Applicat.*, San Diego, CA, Jan. 1994.
[19] D. B. Rutledge, private communication.
[20] J. J. Lee, D. Atkinson, J. J. Lam, L. Hackett, R. Lohr, L. Larson, R. Loo, M. Matloubian, G. Tangonon, H. De Los Santos, and R. Brunner, "MEMS antenna systems: Concepts, design, and system implications," in *Nat. Radio Sci. Meeting*, Boulder, CO, 1996.
[21] J.-M. Karam, *Electron. Design*, July 1998.

Elliott R. Brown (M'92–SM'97), for photograph and biography, see this issue, p. 1820.